Multipeak low-temperature behavior of specific heat capacity in frustrated magnetic systems: An exact theoretical analysis

E. Jurčišinová[1,2] and M. Jurčišin[1,2,3]

[1]*Institute of Experimental Physics, Slovak Academy of Sciences, Watsonova 47, 040 01 Košice, Slovakia*

[2]*Bogoliubov Laboratory of Theoretical Physics, Joint Institute for Nuclear Research, 141 980 Dubna, Moscow Region, Russian Federation*

[3]*Department of Theoretical Physics and Astrophysics, Faculty of Science, P.J. Šafárik University, Park Angelinum 9, 040 01 Košice, Slovakia*

(Received 23 November 2017; published 21 May 2018)

We investigate in detail the process of formation of the multipeak low-temperature structure in the behavior of the specific heat capacity in frustrated magnetic systems in the framework of the exactly solvable antiferromagnetic spin-1/2 Ising model with the multisite interaction in the presence of the external magnetic field on the kagome-like Husimi lattice. The behavior of the entropy of the model is studied and exact values of the residual entropies of all ground states are found. It is shown that the multipeak structure in the behavior of the specific heat capacity is related to the formation of the multilevel hierarchical ordering in the system of all ground states of the model. Direct relation between the maximal number of peaks in the specific heat capacity behavior and the number of independent interactions in studied frustrated magnetic system is identified. The mechanism of the formation of the multipeak structure in the specific heat capacity is described and studied in detail, and it is generalized to frustrated magnetic systems with arbitrary numbers of independent interactions.

DOI: 10.1103/PhysRevE.97.052129

I. INTRODUCTION

One of the most important quantities which is intensively studied and measured in the process of experimental investigation of various frustrated magnetic systems is the specific heat capacity which usually exhibits various anomalies such as, e.g., the appearance of the second peak at low temperatures widely known as the Schottky-type anomaly (see, e.g., Refs. [1–19]). However, besides the most common two-peak Schottky-type anomaly in the low-temperature behavior of the specific heat capacity, there also exist magnetic materials for which more than the two-peak structure of the specific heat capacity is measured (see, e.g., Refs. [20–29]). It is evident that such specific heat capacity behavior means that the corresponding magnetic systems must pass through significant entropy changes since the specific heat capacity is, by definition, directly related to the entropy of the studied system. Here, it is also worth mentioning that the multipeak structure in the temperature behavior of the specific heat capacity is not present in the magnetic systems only but can also be observed in other physical situations, e.g., in the investigation of the specific heat capacity properties of plasma [30].

From phenomenological as well as fundamental points of view, it is therefore desirable and useful to find and describe a general microscopic mechanism which could be responsible for such anomalous behavior of the specific heat capacity in frustrated magnetic systems at low temperatures. For this purpose, it is most convenient to study this behavior of specific heat capacity in the framework of a theoretical model which, on one hand, would be able to describe (at least qualitatively) a realistic frustrated magnetic system and, on the other hand, would be exactly solvable in the presence of the external magnetic field. The last requirement is in fact very important because various anomalous properties of the specific heat capacity are usually observed when a nonzero magnetic field is applied. Unfortunately, the set of even classical exactly solvable spin models on regular lattices is restricted to one- and two-dimensional models [31–34], but at the same time no relevant classical spin model on a regular two-dimensional lattice exists that would be exactly solved in the nonzero external magnetic field. It is therefore evident that for a systematic theoretical investigation of the properties of various frustrated magnetic systems in the presence of the external magnetic field one must necessarily use an approximation which, however, must be chosen in such a way that it takes into account at least the basic properties of the original model responsible for the frustration.

In this respect, as for the geometrically frustrated magnetic systems [35], one such approximation which, on one hand, preserves the basic properties of the model responsible for the geometrical frustration and, on the other hand, allows one to perform an exact analysis of the model, is the approximation based on the well-defined recursive lattices, e.g., on the generalized Bethe lattices known as the so-called Husimi lattices [36–38]. The main advantage of recursive lattices is the fact that various statistical models on such kind of lattices can always be investigated by using the recursive relations technique (see, e.g., Refs. [39–43] and references cited therein). Moreover, in some special cases, models on recursive lattices are also exactly solvable in fully analytic form even in the presence of the external magnetic field [44–46]. Among such exactly solvable models is the antiferromagnetic spin-1/2 Ising model on the corner-sharing triangles recursive lattice with coordination number four, i.e, on the so-called kagome-like Husimi lattice [44,45] (see Fig. 1), which represents an appropriate approximation of the regular two-dimensional kagome lattice shown explicitly in Fig. 2 and which takes into account its basic geometrical structure responsible for strong geometrical frustration.

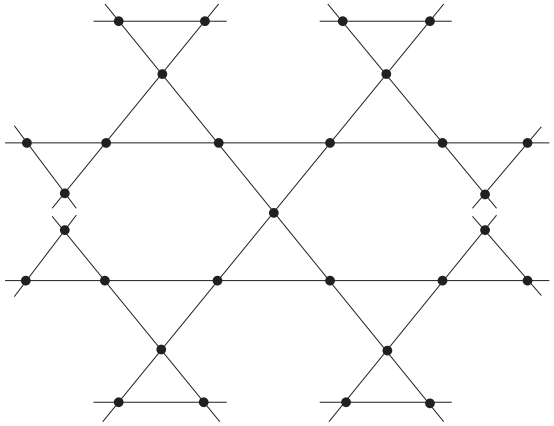

FIG. 1. The structure of the kagome-like Husimi recursive lattice.

However, the fact that the antiferromagnetic spin-1/2 Ising model on the kagome-like Husimi recursive lattice is exactly solvable not only in the presence of the external magnetic field [44] but also when an additional interaction is considered, e.g., when the multisite interaction among spin variables within elementary triangles of the lattice is present [45], gives one other important possibility, namely, the opportunity to investigate systematically the impact of the presence of additional interactions on various properties of geometrically frustrated magnetic systems such as the full system of ground states of the model and the magnetization properties of the model. Namely, these properties were studied in detail in Ref. [45]. In the present paper, in the framework of this exactly solvable model, we will concentrate our attention on the investigation of another important phenomenon related to the frustration, namely, to the aforementioned nontrivial multipeak behavior of the specific heat capacity at low temperatures in frustrated magnetic systems.

It means that our main aim will be to identify on a fundamental level of investigation the source of the multipeak behavior of the specific heat capacity in frustrated magnetic systems in the framework of a well-defined exactly solvable model as well as to understand the process of the very formation of this multipeak structure. As we shall see, the main role in the very existence of this multipeak behavior of the specific heat capacity plays the formation of a nontrivial hierarchical system of highly macroscopically degenerated ground states of the model in the limit $T \to 0$. It will be shown that the strong hierarchies of the residual entropies exist among various neighboring ground states of different orders and that the existence of such multilevel hierarchies of the residual entropies leads to the appearance of the multipeak temperature behavior of the specific heat capacity. As we shall show, the maximal possible number of peaks in the specific heat capacity behavior directly depends on the number of hierarchical levels of the system of the model ground states which, on the other hand, is directly given by dimension of the independent parametric space of the model.

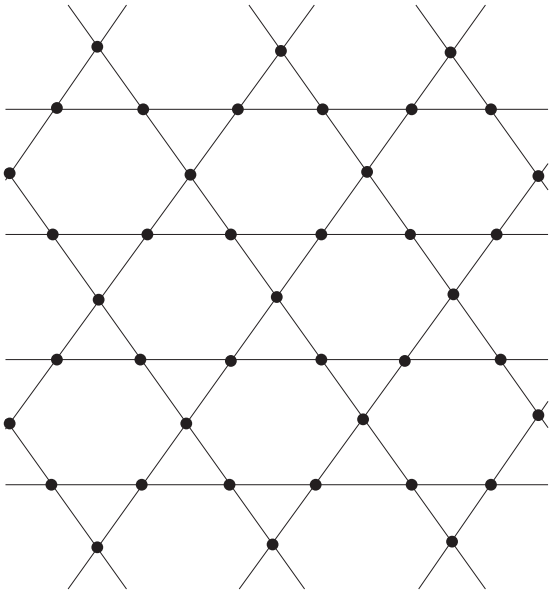

FIG. 2. The structure of the regular kagome lattice.

The paper is organized as follows. In Sec. II, the model is briefly introduced. In Sec. III, the entropy of the model is investigated and the residual entropies of all ground states are found. In addition, their hierarchical ordering is defined and discussed. The multipeak behavior of the specific heat capacity as the function of the temperature under the influence of the presence of the multisite interaction is studied in detail in Sec. IV. Finally, obtained results are briefly reviewed and discussed in Sec. V.

II. DESCRIPTION OF THE MODEL

In what follows, we shall investigate the influence of the multisite interaction among spin variables within each elementary triangle on the thermodynamical properties of the antiferromagnetic spin-1/2 Ising model in the presence of the external magnetic field on the kagome-like Husimi recursive lattice, i.e., on the recursive lattice built by corner-sharing triangles with coordination number $z = 4$ shown explicitly in Fig. 1. As was already mentioned in the introduction, this recursive lattice represents an adequate approximation of real two-dimensional kagome lattice (Fig. 2) which takes into account its basic geometric structure responsible for frustration [35]. The Hamiltonian of the model has the following form,

$$\mathcal{H} = -J \sum_{\langle i\, j\rangle} s_i s_j - J' \sum_{\langle i\, j\, k\rangle} s_i s_j s_k - H \sum_i s_i, \qquad (1)$$

where each variable s_i acquires one of two possible values ± 1, $J < 0$ is the nearest-neighbor antiferromagnetic interaction parameter, J' represents the multisite interaction among spin variables within single triangles, and H is the external magnetic field. Thus, the first sum in Eq. (1) runs over all nearest-neighbor spin pairs, the second sum runs over all elementary triangles, and the third sum runs over all spin sites.

As with any statistical model on a recursive lattice, the above-defined model can be studied numerically by using the standard recursion relations technique (see, e.g., Ref. [32]). But, as was shown in detail in Refs. [44,45], the exact solution of the model exists without as well as with the presence of the multisite interaction. In Ref. [45], it was proven that the model exhibits a unique solution for all values of the model parameters and the explicit analytical form of the corresponding

unique stable fixed point of the recursion relations was found which completely drives the model thermodynamics. Using this solution, the influence of the multisite interaction on the magnetization properties of the model was investigated and the system of all ground states of the model was found and their exact values of magnetization were determined. The most important conclusion obtained in Refs. [44,45] is the fact that, along with the standard plateau ground states, the model also exhibits the existence of well-defined so-called single-point ground states which, depending on the values of the model parameters, are realized for exactly defined values of the external magnetic field.

The aim of the present paper is to use the nontrivial fact of the existence of the exact solution of the model to perform detailed analysis of its thermodynamics and to determine the role of the multisite interaction in the low-temperature properties of the model. The main attention is devoted to the investigation of the low-temperature behavior of the specific heat capacity of the model related to the presence of the multisite interaction to understand in general the role of additional interactions in frustrated magnetic systems for the very existence of various specific heat capacity anomalies as well as their properties. To this end, it is necessary first to investigate the entropy of the model, which is performed in detail in the next section.

III. ENTROPY AND RESIDUAL ENTROPIES OF ALL GROUND STATES OF THE MODEL

The entropy per site s of a given model can be determined by using the free energy per site f through the standard relation

$$s = -\frac{\partial f}{\partial T}. \tag{2}$$

The free energy per site of the present model can be derived, e.g., by using techniques described in Refs. [47,48] and has the form [49]

$$\begin{aligned}\beta f = {} & \tfrac{1}{3}\ln(x^3 e^{3h+3K+K'} + 3x^2 e^{h-K-K'} \\ & + 3x e^{-h-K+K'} + e^{-3h+3K-K'}) \\ & - \ln(x^2 e^{2h-K-K'} + 2x e^{K'-K} + e^{-2h+3K-K'}),\end{aligned} \tag{3}$$

where $\beta = 1/(k_B T)$, T is the temperature, k_B is the Boltzmann constant, $K = \beta J$, $K' = \beta J'$, $h = \beta H$, and x is the exact solution of the corresponding recursion relation obtained in Ref. [45] which has the following explicit form

$$x = \frac{1}{3a}\left[-b - \frac{2^{1/3}(3ac - b^2)}{B} + \frac{B}{2^{1/3}}\right], \tag{4}$$

where

$$\begin{aligned}B = {} & [27a^2 d - 2b^3 + 9abc \\ & + \sqrt{4(3ac - b^2)^3 + (27a^2 d - 2b^3 + 9abc)^2}]^{1/3}\end{aligned} \tag{5}$$

and

$$a = e^{4h}, \tag{6}$$

$$b = e^{2K'}(2e^{2h} - e^{4(h+K)}), \tag{7}$$

$$c = e^{4K} - 2e^{2h}, \tag{8}$$

$$d = e^{2K'}. \tag{9}$$

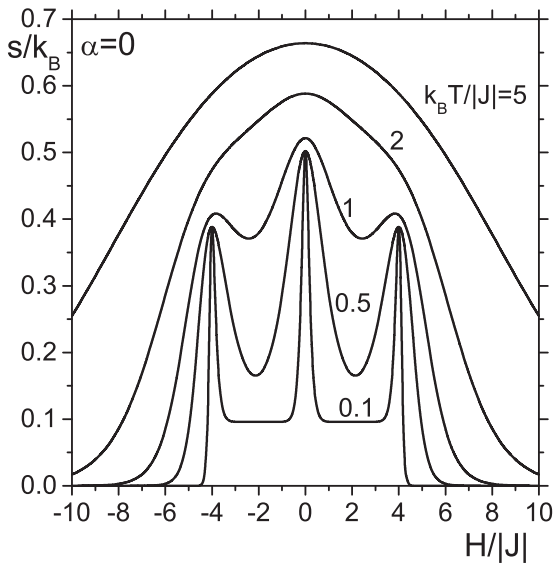

FIG. 3. Dependence of the entropy per site on the external magnetic field for various nonzero values of the reduced temperature for $\alpha = 0$.

The explicit expression for the entropy per site of the studied model is relatively large. Nevertheless, for completeness, it can be found in the appendix.

Depending on the value of the ratio $\alpha = J'/|J|$, the studied model exhibits three qualitatively different behaviors of the entropy as the function of the reduced temperature and of the external magnetic field depicted in Figs. 3–5 for three typical values of the parameter α, namely, for $\alpha = 0, 1$, and 2. First of all, Fig. 3 (where the dependence of the entropy per site on the external magnetic field for various values of the temperature is shown for $\alpha = 0$, i.e., in the case when the multisite interaction is absent at all) represents a typical qualitative behavior of the entropy per site for $-1 < \alpha < 1$. Here, the formation of the corresponding system of residual entropies of the ground states of the model in the limit $T \to 0$ can be seen. On the other hand, when the absolute value of the multisite interaction is exactly equal to the absolute value of the nearest-neighbor antiferromagnetic interaction, i.e., for $|\alpha| = 1$, the behavior of the entropy changes qualitatively and is demonstrated in Fig. 4 for $\alpha = 1$. Note that the corresponding figure for $\alpha = -1$ can be obtained from Fig. 4 by the reflection with respect to $H = 0$ axis. The third typical situation which holds for $|\alpha| > 1$ is shown in Fig. 5 for $\alpha = 2$. Here again, the corresponding dependence of the entropy for negative values of α is obtained by simple reflection with respect to $H = 0$ axis.

From all these figures, it is evident that the plateau ground states (except of the saturated ground states with $|m| = \pm 1$) as well as the single-point ground states, which are formed on the borders between corresponding plateau-like ground states, acquire nonzero residual entropies in the limit $T \to 0$. As was shown in Ref. [45], where the magnetization properties of the model were investigated, the "phase" diagram of the ground states of the model in $H/|J|$ versus α plane consists of four plateau-like ground states with values of the magnetization $m = \pm 1/3$ and ± 1 and the corresponding system of the single-point ground states which are shown explicitly in Fig. 6.

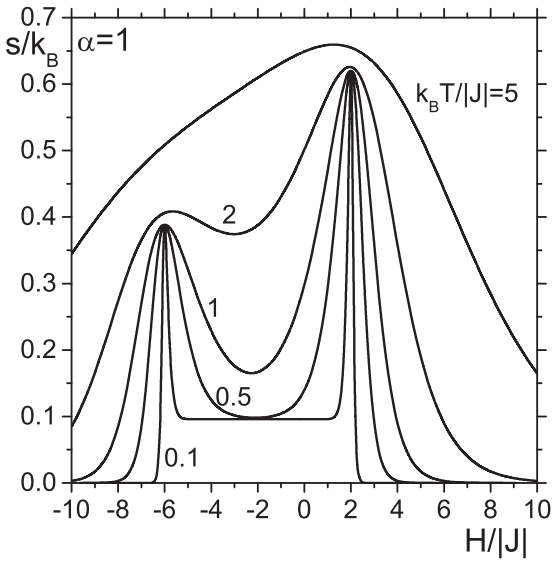

FIG. 4. Dependence of the entropy per site on the external magnetic field for various nonzero values of the reduced temperature for $\alpha = 1$.

The formation of the system of nonzero residual entropies for all nontrivial ground states of the model means that all of them are highly macroscopically degenerated. Let us remember that the macroscopic degeneracy Ω of a given state of the system with total number of sites N is related to the total entropy $S = Ns$ by the relation $S = k_B \ln \Omega$.

It follows from Fig. 6 that the model exhibits two nontrivial plateau ground states with $m = \pm 1/3$. Their residual entropy is equal to

$$s = \frac{k_B}{3} \ln \frac{4}{3} \approx 0.095894\, k_B. \tag{10}$$

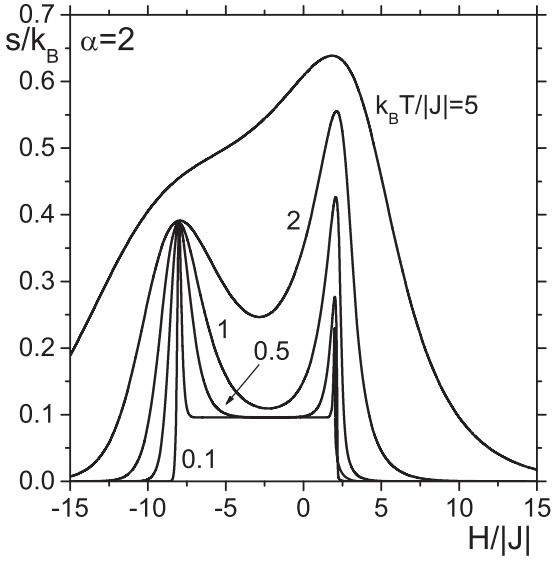

FIG. 5. Dependence of the entropy per site on the external magnetic field for various nonzero values of the reduced temperature for $\alpha = 2$.

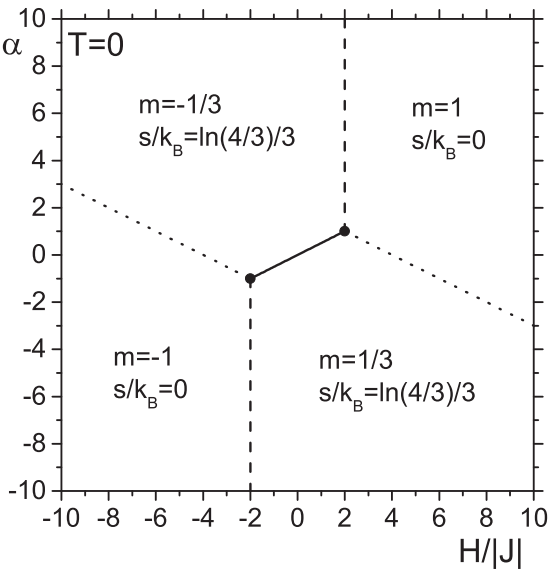

FIG. 6. The ground-state phase diagram of the model in the $H/|J|$ vs α plane. The values of the magnetization and of the residual entropies of the plateau ground states are written explicitly. On the other hand, the values of the magnetization and the residual entropies of the single-point ground states are the following: $m = 0$ and $s \approx 0.501359\, k_B$ (the solid line), $m = 0$ and $s \approx 0.231049\, k_B$ (the dashed lines), $m = \pm 0.6$ and $s \approx 0.387717\, k_B$ (the dotted lines), and $m \approx \pm 0.217208$ and $s \approx 0.619621\, k_B$ (the filled circles).

The model also exhibits the existence of four thermodynamically different single-point ground states. Three of them are realized on the corresponding lines in $H/|J|$ versus α plane and separate various neighboring plateau-like ground states (see Fig. 6). It follows from Figs. 3–5 that all of them are considerably more macroscopically degenerated in comparison to the plateau-like ground states. Here, it is important to stress that the model exhibits the existence of two qualitatively different single-point ground states which are realized on the corresponding lines in the plane $H/|J|$ versus α (solid and dashed lines in Fig. 6) and which have the same value of the magnetization, namely, $m = 0$. It means that although from a pure magnetization point of view these single-point ground states seem to be equivalent, nevertheless their thermodynamics are different. The first of them is realized on the line $H/|J| = 2\alpha$ for $-1 < \alpha < 1$ (the solid line in Fig. 6) and represents the separating ground state between plateau ground states with values of magnetization $m = \pm 1/3$. Its residual entropy is the following:

$$s = \frac{k_B}{3} \ln \frac{9}{2} \approx 0.501359\, k_B. \tag{11}$$

It is worth mentioning here that this residual entropy is very close to the residual entropy of the same ground state on the regular kagome lattice at zero external magnetic field, which was found in Ref. [50], and its approximate value is $s \approx 0.50183 k_B$. It means that our recursive model describes the thermodynamics of the model on the real kagome lattice very well, not only on the qualitative level but also on the quantitative level.

The second thermodynamically different single-point ground state with zero value of magnetization is realized on the lines $H/|J| = \pm 2$ for $\alpha > 1$ and $\alpha < -1$, respectively, which separate the plateau-like ground states with $m = \pm 1/3$ and the corresponding saturated ground states with $m = \pm 1$ (the dashed lines in Fig. 6). The exact value of the residual entropy is now given as follows:

$$s = \frac{k_B}{3} \ln 2 \approx 0.231049\, k_B. \tag{12}$$

It is evident that the residual entropy of this single-point ground state is much smaller than the residual entropy of the single-point ground state with the same magnetization discussed above. It means that, from a thermodynamical point of view, they represent two qualitatively different ground states with significantly different macroscopic degeneracies; i.e., they are formed by nonequal sets of possible spin configurations.

The last line-like single-point ground states are realized on lines $H/|J| = \pm 4 - 2\alpha$ for $\alpha < 1$ and $\alpha > 1$, respectively (the dotted lines in Fig. 6) and have the absolute value of the magnetization $|m| = 0.6$. Their residual entropy is equal to

$$s = \frac{k_B}{3} \ln \frac{16}{5} \approx 0.387717\, k_B. \tag{13}$$

Besides, as follows from Fig. 6, the model also exhibits the existence of totally unique single-point ground states which are realized at two points at which three plateau-like ground states meet and, at the same time, at which all three different line-like single-point ground states meet, i.e., for $|H/J| = \pm 2$ and $\alpha = \pm 1$ (the filled circles in Fig. 6). The nontrivial exact expression for their absolute value of the magnetization was found in Ref. [45]. The approximate absolute value of the magnetization of these single-point ground states is $|m| \approx 0.217208$ and their residual entropy is given as follows:

$$s = \frac{k_B}{3} \ln \frac{y^2(2+y)^3}{y(3+y)+3} \approx 0.619621\, k_B, \tag{14}$$

where

$$y = \frac{7^{1/3} w^2 - w + 7^{2/3}}{3w}, \quad w = \left(\frac{1 + 3i\sqrt{3}}{2} \right)^{1/3}. \tag{15}$$

Note that these single-point ground states are the most macroscopically degenerated ground states of the model. At the same time, let us note that their residual entropy is relatively close to the maximal possible entropy of any two-state spin system in the limit $T \to \infty$ which is equal to $s_{\max} = k_B \ln 2 \approx 0.693147 k_B$. As we shall see, these single-point ground states are unique not only in the sense that they are maximally macroscopically degenerated ground states of the model but also in the sense that their existence causes nontrivial anomaly behavior of the specific heat capacity in their vicinity.

It follows from the above discussion that from the point of view of their dimensionality the studied magnetic system in fact exhibits the existence of three different types of ground states. First are the standard plateau-like ground states which are realized in the corresponding two-dimensional regions of the two-dimensional parametric space of the model at zero temperature given by two dimensionless parameters $H/|J|$ and $\alpha = J'/|J|$ (see Fig. 6). This type of ground state is realized in the regions with maximal dimension in given independent parametric space. At the same time, however, in our case, there exist two types of the so-called single-point ground states, i.e., the ground states which are realized at exactly defined values of the external magnetic field $H/|J|$ for given concrete values of the other model parameters (in our case for given value of the parameter α). All of them correspond to objects with smaller dimensions in the parameter space of the model. In our case, we have single-point ground states which are realized on lines in the two-dimensional parameter space, i.e., are one-dimensional objects, and we also have the single-point ground states which are realized at unique points of the parameter space, i.e., they are the ground states with zero dimension in the parametric space of the model (see Fig. 6).

Thus, one can observe a well-defined hierarchy in the set of all ground states of the model based on their dimensionality in the parametric space. As a result, in our case, the set of all ground states is divided into three disjunct subsets containing the corresponding ground states of the same order (dimensionality). If we denote the set of all ground states in the framework of our two parametric model as G_2, then it is evident that one can write the following simple relation $G_2 = G_{2,0} \bigcup G_{2,1} \bigcup G_{2,2}$, where $G_{2,i}, i = 0,1,2$ are the disjunct subsets of the ground states with the same dimensionality equal to i. In what follows, the elements of the set $G_{2,i}$ will be called as the ground states of ith order. At the same time, each ground state can be associated with the corresponding region in the two-dimensional parameter space in which this ground state is realized. Therefore, if we denote whole two-dimensional parametric space at zero temperature as $\mathcal{G}_2$ then it is evident that one can also write $\mathcal{G}_2 = \mathcal{G}_{2,0} \bigcup \mathcal{G}_{2,1} \bigcup \mathcal{G}_{2,2}$, where $\mathcal{G}_{2,i}$ are regions in which ground states $G_{2,i}$ are realized. In our case, the sets $\mathcal{G}_{2,i}$ are also disjunct as a result of the fact that the model does not exhibit coexistence of the phases, i.e., that we have unique solution for all values of the parameters of the model [45].

This classification can be extended to the general case of a frustrated classical magnetic system with n different couplings $J_1, \ldots, J_n$ in the external magnetic field H. In this general case, one can define, without loss of generality, the following set of n independent dimensionless parameters: $J_2/J_1, J_3/J_1, \ldots, J_n/J_1, H/J_1$, which define the n-dimensional parametric space of the model at zero temperature, i.e., the parametric space of the ground states of the model. As a result, in general, the set of all ground states G_n of this model will consist of the subset $G_{n,n}$ of all plateau-like ground states with dimensionality n, i.e., which are realized in the n-dimensional regions in the ground-state parametric space, and all subsets of various single-point ground states $G_{n,i}, i = 0, \ldots, n-1$ of all smaller orders, i.e., $G_n = \bigcup_{j=0}^{n} G_{n,j}$. In addition, one can again write $\mathcal{G}_n = \bigcup_{j=0}^{n} \mathcal{G}_{n,j}$, where $\mathcal{G}_{n,j}$ represents all regions in which ground states $G_{n,j}$ of jth order are realized (which are all disjunct if the model exhibits a unique solution regardless of the parameter values at zero temperature) and $\mathcal{G}_n$ represents an n-dimensional independent parametric space of the model at zero temperature.

It is important to stress that if the model exhibits a single unique solution for all parameter values at zero temperature, then every ground state of the order $i = 0, 1, \ldots, n-1$ separates corresponding neighboring ground states of the order

$i+1$ (see Fig. 6). At the same time, due to the fundamental thermodynamic law that the entropy is always an increasing function of the temperature, the following assertion must be valid: For arbitrary two neighboring ground states of different orders the residual entropy of the ground state of higher order is lower or at most equal to the residual entropy of the lower order ground state. As we shall see, this multilevel cascade hierarchy of the macroscopic degeneracy of the neighboring ground states plays the central role for understanding and natural explanation of experimentally measured anomalous behavior of the specific heat capacity at low temperatures such as the existence of a multipeak structure of the specific heat capacity in various frustrated magnetic systems.

It is also necessary to note that a similar idea of the existence of hierarchical ordering of all ground states was also proposed and discussed in the framework of the spin configuration analysis of the various Ising-like models on geometrically frustrated lattices [51–54].

IV. HIERARCHY OF GROUND STATES AND LOW-TEMPERATURE MULTIPEAK STRUCTURE OF THE SPECIFIC HEAT CAPACITY

As was already mentioned, the main aim of the present paper is to investigate in detail the low-temperature anomaly behavior of the specific heat capacity in frustrated systems and to identify its source in the magnetic systems with additional interactions which are represented by the multisite interaction in the framework of the studied exactly solvable antiferromagnetic frustrated model.

By definition, the specific heat capacity at the constant external magnetic field is related to the entropy per site or directly to the free energy per site as follows:

$$c_H = T\left(\frac{\partial s}{\partial T}\right)_H = -T\left(\frac{\partial^2 f}{\partial T^2}\right)_H. \tag{16}$$

Note that having the exact expression for the free energy per site for the studied model given in Eq. (3) means that the exact expression for the specific heat capacity can be immediately derived. For completeness, its explicit form is shown in the appendix. The fact that in the present model the exact expression for the specific heat capacity exists even in the nonzero external magnetic field is quite exceptional in the framework of classical models of the statistical mechanics. This allows us to perform an exact analysis of its properties and to understand peculiarities in its behavior on a fundamental theoretical level.

Detailed analysis of the temperature dependence of the specific heat capacity shows that its behavior strongly depends on the value of the external magnetic field $H/|J|$ as well as on the strength of the multisite interaction in comparison to the nearest neighbor antiferromagnetic coupling constant represented by the parameter $\alpha = J'/|J|$.

A. The specific heat capacity behavior for $\alpha = 0$

First of all, in the case when the multisite interaction is not present, depending on the value of the external magnetic field, the studied model exhibits the standard one-peak behavior of the specific heat capacity as well as the two-peak behavior

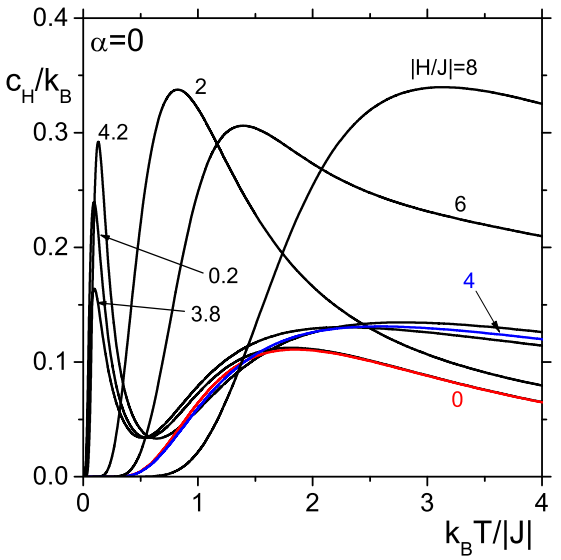

FIG. 7. The behavior of the specific heat capacity as the function of the reduced temperature for various absolute values of the external magnetic field for $\alpha = 0$.

with appearance of the second so-called Schottky-type peak at low temperatures. The behavior of the specific heat capacity as the function of the reduced temperature for $\alpha = 0$ and for various absolute values of the external magnetic field is shown explicitly in Fig. 7. As follows from this figure, in this case, the Schottky-type anomaly behavior of the specific heat capacity appears in the left as well as right vicinity of the values of the external magnetic field for which the corresponding single-point ground states are formed in the limit $T \to 0$, i.e., in the vicinity of $H/|J| = 0$ and ± 4 (the curves for $|H/J| = 0.2, 3.8$, and 4.2 in Fig. 7). Note also that directly at the absolute values of the external magnetic field for which the single-point ground states are formed the specific heat capacity has standard one-peak behavior [see the curves for $|H/J| = 0$ (dash-dotted red curve) and $|H/J| = 4$ (dashed blue curve) in Fig. 7].

The properties of the Schottky-type anomaly behavior of the specific heat capacity near the corresponding single-point ground-state values of the external magnetic field are shown in detail in Fig. 8. Here, it is again evident that the specific heat capacity has standard one-peak behavior as the function of the temperature for the absolute values of the magnetic field for which the single-point ground states are formed, i.e., for $|H/J| = 0$ and 4 (see the corresponding black curves in Fig. 8). Note that these peaks are also common for the specific heat capacity curves for the magnetic fields from the left as well as right vicinity of the corresponding single-point values of the external magnetic field. At the same time, one can see that the second (Schottky) peaks for the absolute values of the magnetic field from the same side of a given single-point value of the magnetic field have similar heights and shift toward zero temperature when the absolute value of the magnetic field approaches the corresponding single-point value of the external magnetic field, i.e., the value of the external magnetic field at which the corresponding single-point ground state is formed in the limit $T \to 0$ (in what follows, we shall usually use the reduced version of this phrase for shortness).

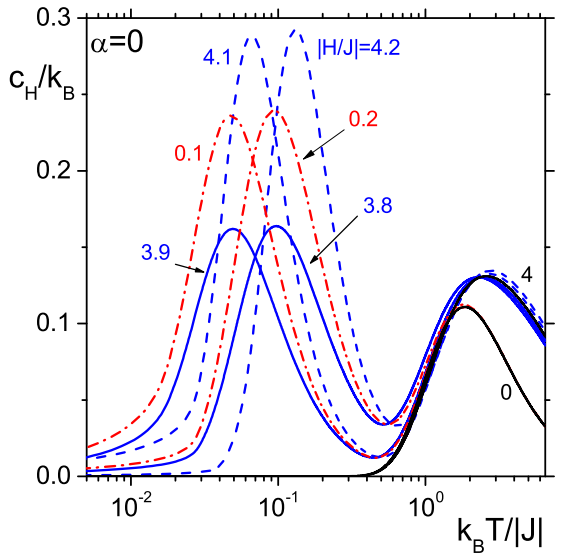

FIG. 8. The behavior of the specific heat capacity as the function of the temperature in the vicinity of the single-point ground-state absolute values of the external magnetic field $|H/J| = 0$ and 4 for $\alpha = 0$.

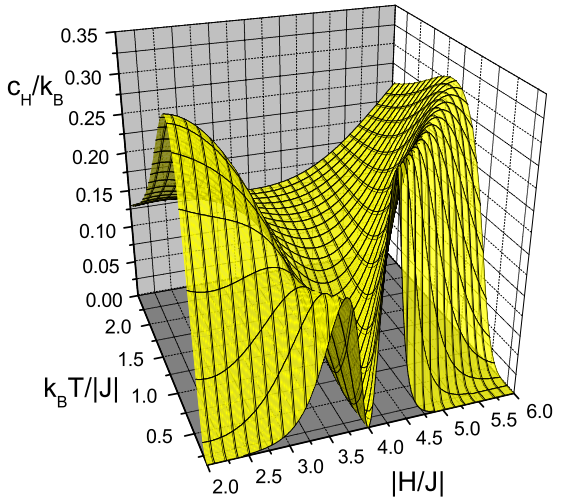

FIG. 10. The behavior of the specific heat capacity as the function of the temperature and of the absolute value of the external magnetic field for $\alpha = 0$ in the vicinity of $|H/J| = 4$ for which the single-point ground state is formed in the limit $T \to 0$. The formation of the Schottky peaks in the left and right vicinity of $|H/J| = 4$ is shown explicitly.

Note also that the Schottky peaks from the vicinity of different absolute values of the single-point ground state magnetic field have considerably different heights. Besides, the heights of the Schottky peaks from the left and right vicinity of the absolute value of the magnetic field $|H/J| = 4$ are also different (see the corresponding curves for $|H/J| = 3.8$,3.9 and 4.1,4.2 in Fig. 8). All these facts are directly related to different differences between the residual entropies of the corresponding single-point ground state and the neighboring plateau ground-state formation, which in the limit $T \to 0$ can be seen explicitly in Fig. 9, where the behavior of the entropy as the function of the temperature is shown for the same absolute values of the external magnetic field as in Fig. 7. Finally, the behavior of the specific heat capacity as a function of the temperature and the external magnetic field in the vicinity of the single-point value of the external magnetic field $|H/J| = 4$ for $\alpha = 0$ is demonstrated explicitly in Fig. 10 with clear illustration of the formation of the Schottky-type peak at low temperatures. At the same time, the formation of the field-induced sharp double-peak structure in the behavior of the specific heat capacity at low temperatures centered in the absolute value of external magnetic field for which the single-point ground state is formed can also be seen explicitly in Fig. 10.

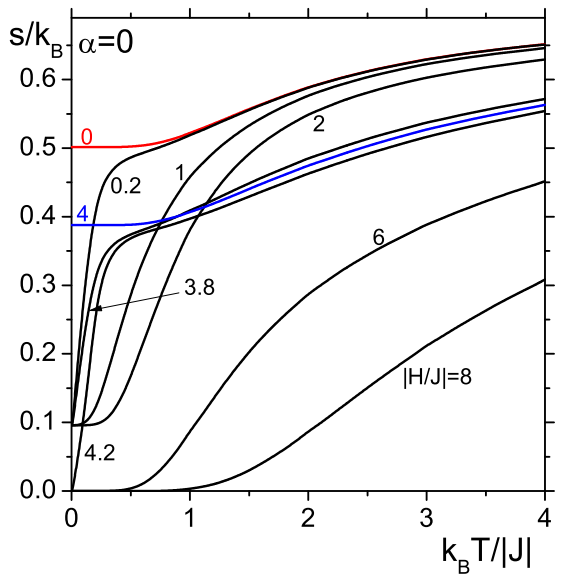

FIG. 9. The dependence of the entropy per site on the reduced temperature for $\alpha = 0$ and for the same absolute values of the external magnetic field as in Fig. 7.

Finally, it is worth mentioning that the Schottky peaks in the behavior of the specific heat capacity at low temperatures are formed only in restricted intervals of the absolute values of the external magnetic field, namely, in the interval $0 < |H/J| < 0.606$ in the vicinity of $H = 0$ and in the intervals $3.250 < |H/J| < 4$ and $4 < |H/J| < 5.076$ in the vicinity of $|H/J| = 4$.

B. Influence of multisite interaction on the specific heat capacity anomalies

If one considers pure antiferromagnetic model, i.e., without the presence of the multisite interaction, then the ground-state parametric space, i.e., the parametric space at zero temperature, is one dimensional and given by the only independent dimensionless parameter $H/|J|$. Therefore, in this case, the set of all ground states is $G_1 = G_{1,0} \bigcup G_{1,1}$, where the subset of the zero-order ground states $G_{1,0}$ consists of three single-point ground states realized for $H/|J| = 0, \pm 4$ (geometrically they form the subset $\mathcal{G}_{1,0}$ of the one-parametric space $\mathcal{G}_1$) and the subset of the first-order ground states $G_{1,1}$ consists of the plateau-like ground states with values of the magnetization $m = \pm 1/3, \pm 1$ which geometrically form the subset $\mathcal{G}_{1,1}$. Note that $\mathcal{G}_1 = \mathcal{G}_{1,0} \bigcup \mathcal{G}_{1,1}$. Here, as for the temperature-specific

heat capacity behavior, one can observe only two possible qualitatively different behaviors, namely, the standard one-peak or anomalous two-peak (Schottky) behavior. However, as was already discussed above, the two peaks in the behavior of the specific heat capacity take place only in restricted vicinities of the values of the magnetic field for which the zero-order (single-point) ground states are realized.

When the presence of the multisite interaction is considered in the model, then the ground state parametric space becomes two-dimensional, denoted as $\mathcal{G}_2$ in Sec. III, and is defined by two independent dimensionless parameters $\alpha = J'/|J|$ and $H/|J|$. As follows from Fig. 6, when the multisite interaction is switched on, the positions of the single-point ground states depend of the value of the parameter α, and when the strength of the multisite interaction is equal or larger than the nearest neighbor antiferromagnetic interaction, then even new single-point ground states appear. It is, however, important to realize that the hierarchy of the ground states is also changed. On one hand, the plateau-like ground states $G_{1,1}$ are now realized in two-dimensional regions $\mathcal{G}_{2,2}$ and therefore belong to the subset of the second-order ground states $G_{2,2}$ and the single-point ground states $G_{1,0}$ are now realized on the corresponding lines $\mathcal{G}_{2,1}$; i.e., they also increase their order and now belong to the subset of the first-order ground states $G_{2,1}$. On the other hand, a new subset of the zero-order single-point ground states $G_{2,0}$ emerges here which is realized at unique points (and therefore forms the subset $\mathcal{G}_{2,0}$) in the two-dimensional ground-state parametric space (the filled circles in Fig. 6).

Thus, introducing a new interaction into the model increases the dimension of the ground-state parametric space of the model with appearance of new ground states as well as with appearance of a new ground-state hierarchy. As we shall see, this hierarchical layering of the set of all ground states of the model has a direct relation to the very existence of the multipeak structure as well as to the possible maximal number of peaks in the specific heat capacity behavior at low temperatures.

As was mentioned above, for $\alpha = 0$ the specific heat capacity exhibits the standard one-peak temperature behavior directly at the single-point ground-state values of the external magnetic field, i.e., at $H/|J| = 0, \pm 4$. When the multisite interaction is switched on, the positions of these (first-order) single-point ground states change (see the solid and dotted lines in Fig. 6) but the specific heat capacity persists to exhibit the standard one-peak behavior [the solid black curves in Fig. 11, where the temperature behavior of the specific heat capacity on the line of the first-order single-point ground states is demonstrated for the single-point ground state with $m = 0$, which is realized on the line $H/|J| = 2\alpha$ for $|\alpha| < 1$ (solid line in Fig. 6)]. The situation is changed when, depending on the corresponding line of the single-point ground states, the absolute value of the parameter α obtains some specific value. For the first-order single points on the line $H/|J| = 2\alpha$ for $|\alpha| < 1$, this specific absolute value of the parameter α is $|\alpha| \approx 0.627$. Starting from this absolute value of the parameter α, the system starts to exhibit the Schottky-type anomaly behavior of the specific heat capacity with two-peak structure (see the dashed red curves in Fig. 11). This behavior holds up to $|\alpha| = 1$ and $|H/J| = 2$ where the zero-order single-point ground state with considerably larger residual entropy appears (see the previous

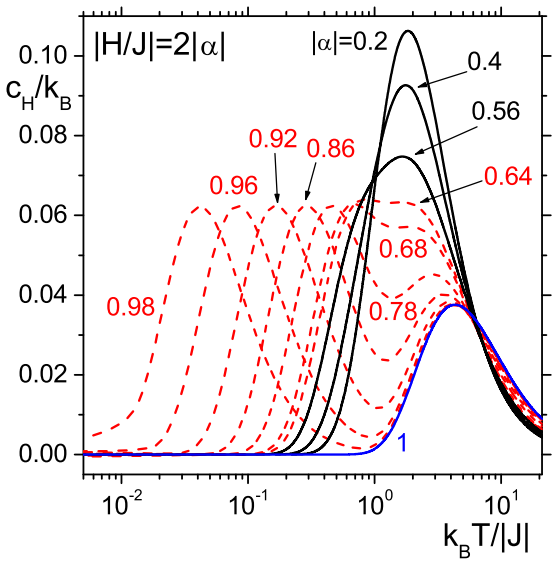

FIG. 11. The dependence of the specific heat capacity on the reduced temperature for various absolute values of the parameter $|\alpha| < 1$ and $|H/J| = 2|\alpha|$, i.e., for parameters of the model for which the corresponding single-point ground state of the first order is realized. The dashed red lines represent the specific heat capacity curves with Schottky-type anomaly behavior. The temperature dependence of the specific heat capacity for parameters $|\alpha| = 1$ and $|H/J| = 2$ at which the zero-order single-point ground state is realized is also shown for comparison (the solid blue line).

section). Note that directly at this single-point ground state of the zero order the specific heat capacity as the function of the temperature has only one peak (the solid blue curve in Fig. 11). As follows from Fig. 11, the height of the Schottky peak (in the interval of the parameters where this type of peak exists at all) is almost constant (see the dashed red curves in Fig. 11). At the same time, the disappearance of the Schottky peak for the corresponding values of the parameters on the line $H/|J| = 2\alpha$ for $|\alpha| < 1$, namely, for $|H/J| = 1.254$ and $|\alpha| = 0.627$, is accompanied by adequate growth of the remaining standard peak of the specific heat capacity. Besides, it is also evident that the Schottky peak shifts toward zero temperature in the limit $|\alpha| \to 1$ on this line and disappears directly at $|\alpha| = 1$, i.e., directly at the point at which the corresponding zero-order ground state is realized in the limit $T \to 0$.

This behavior of the specific heat capacity on the line $H/|J| = 2\alpha$ for $|\alpha| < 1$ shown in Fig. 11 can be explained by the behavior of the entropy, which is explicitly demonstrated in Fig. 12. As follows from this figure, the key role is played by the nearby presence of the highly macroscopically degenerated single-point ground state of the zeroth order at the point $|\alpha| = 1$ and $|H/J| = 2$, residual entropy of which is higher than the residual entropy of the first-order ground state, which is realized on the line $H/|J| = 2\alpha$ for $|\alpha| < 1$ and which has a significant impact on the behavior of the entropy per site in its vicinity with significant slowing down of the entropy reduction in some temperature interval which enlarges toward zero temperature with approaching the model parameters for which the zero-order single-point ground state is formed (see the dashed red curves in Fig. 12).

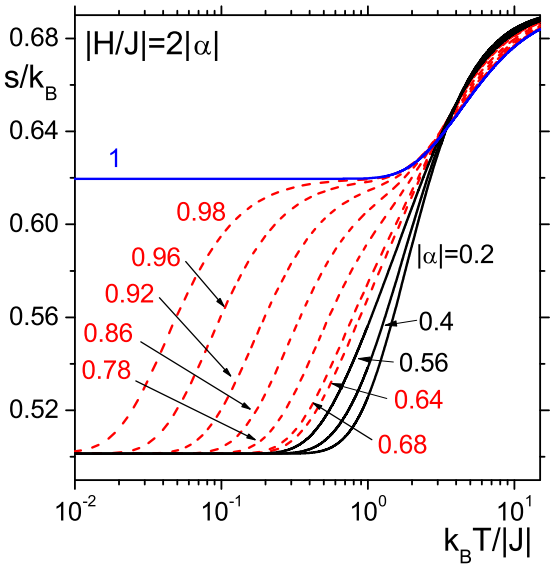

FIG. 12. The dependence of the entropy per site on the temperature for various absolute values of the parameter α $|\alpha| < 1$ and $|H/J| = 2|\alpha|$. The dashed red lines represent the entropy curves for the model parameters for which the Schottky-type anomaly behavior of the specific heat capacity exists (see Fig. 11). The entropy curve for the parameter values $|\alpha| = 1$ and $|H/J| = 2$ for which the residual entropy of the zero-order single-point ground state is realized is also shown for comparison (the solid blue line).

As follows from Figs. 13 and 14, similar behavior of the specific heat capacity can also be seen on the lines of the values of the model parameters on which the first-order single-point

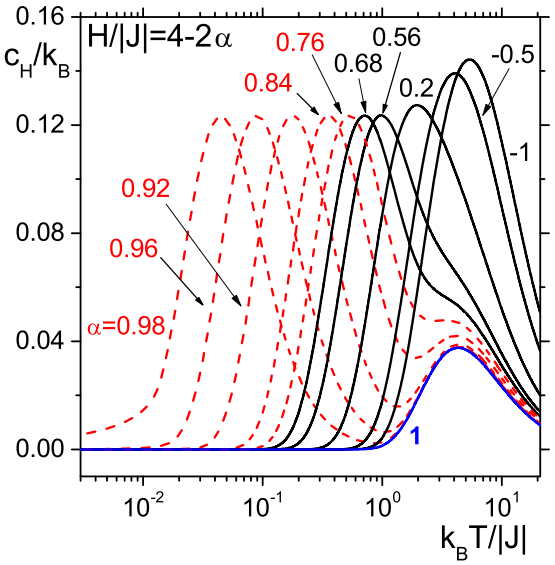

FIG. 13. The dependence of the specific heat capacity on the reduced temperature for various absolute values of the parameter $\alpha > 1$ and $H/|J| = 4 - 2\alpha$, i.e., for parameters of the model at which the corresponding single-point ground state of the first order is realized. The dashed red lines represent the specific heat capacity curves with Schottky-type anomaly behavior. The temperature dependence of the specific heat capacity for parameters $|\alpha| = 1$ and $|H/J| = 2$ at which the zero-order single-point ground state is realized is also shown for comparison (the solid blue line).

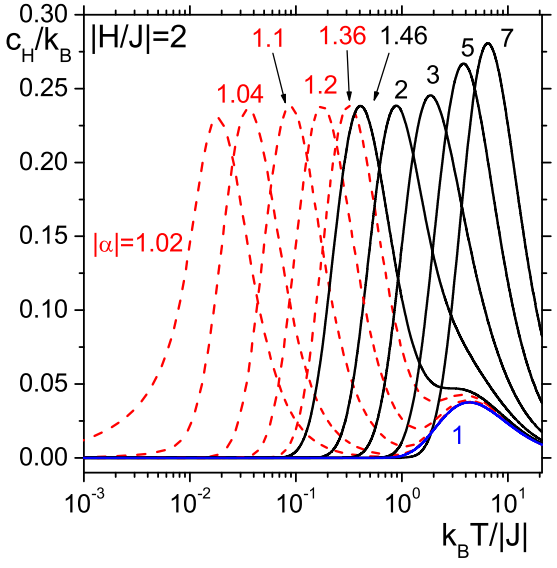

FIG. 14. The dependence of the specific heat capacity on the reduced temperature for various absolute values of the parameter $|H/J| = 2$ for $|\alpha| > 1$, i.e., for parameters of the model at which the corresponding single-point ground state of the first order is realized. The dashed red lines represent the specific heat capacity curves with Schottky-type anomaly behavior. The temperature dependence of the specific heat capacity for parameters $|\alpha| = 1$ and $|H/J| = 2$ at which the zero-order single-point ground state is realized is also shown for comparison (the solid blue line).

ground states with values of the magnetization $m = \pm 0.6$ are realized, i.e., on lines $H/|J| = \pm 4 - 2\alpha$ for $\alpha < 1$ and $\alpha > -1$, respectively, as well as on the lines $H/|J| = \pm 2$ for $\alpha > 1$ and $\alpha < -1$, respectively, on which new first-order single-point ground states are realized with zero magnetization (see Fig. 6). Detailed analysis shows that, in these cases, the Schottky-type behavior of the specific heat capacity with two-peak structure is realized on the lines $H/|J| = \pm 4 - 2\alpha$ for $0.753 < \alpha < 1$ and $-1 < \alpha < -0.753$, respectively, as well as on the lines $H/|J| = \pm 2$ for $1 < \alpha < 1.451$ and $-1.451 < \alpha < -1$, respectively (see also the dashed red lines in Figs. 15 and 16).

It is worth mentioning here that while the heights of the Schottky peaks, which are realized on the corresponding different lines of the single-point ground states, are different (which is related to the different values of the residual entropies of these ground states), the standard peak (the first peak) in the specific heat capacity is common for all of them with the same height as well as with the same position and, at the same time, is also identical to the only peak in the specific heat capacity behavior for parameters $|\alpha| = 1$ and $|H/J| = 2$ for which the zero-order singe-point ground states are realized (see the dashed red and solid blue curves in Figs. 11, 13, and 14). This behavior is related to the fact that this common standard peak in the specific heat capacity is a result of the process of formation of the residual entropy of the corresponding central zero-order single-point ground state at $|H/J| = 2$ and $|\alpha| = 1$ from fully disordered state at high temperatures which is common for all of them.

Thus, we can conclude that while for the parameter values for which the zero-order single-point ground states are realized

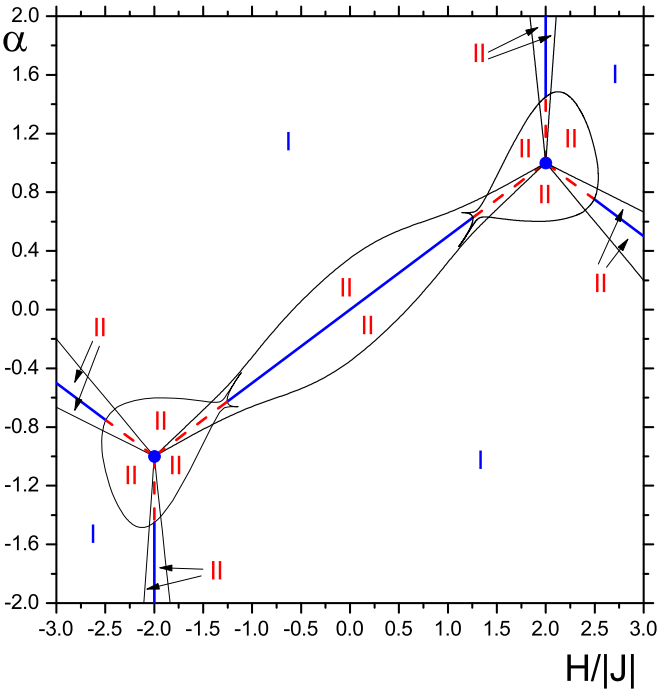

FIG. 15. The regions of the parameters of the model for which the specific heat capacity exhibits one-peak (the blue filled circle, the blue lines, and the two-dimensional regions denoted by blue roman numeral I), two-peak (the dashed red lines and the two-dimensional regions denoted by red roman numeral II), and three-peak (not denoted explicitly in the figure) behavior as the function of the temperature. The three-peak specific heat capacity regions, which can be also seen but are too small to be denoted here, are shown explicitly in Fig. 16, where they are denoted by green roman numeral III.

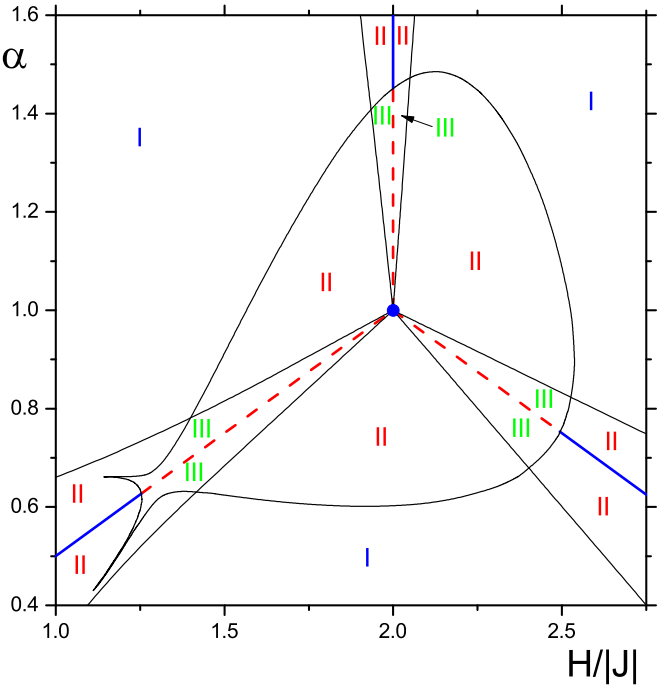

FIG. 16. Detailed illustration of the regions of the model parameters for which the specific heat capacity exhibits one-peak (the blue filled circle, the blue lines, and the two-dimensional regions denoted by blue roman numeral I), two-peak (the dashed red lines and the two-dimensional regions denoted by red roman numeral II), and three-peak (the two-dimensional regions denoted by the green roman numeral III) behavior as the function of the temperature.

($H/|J| = \pm 2$ and $\alpha = \pm 1$) the model exhibits only standard one-peak behavior of the specific heat capacity as the function of the temperature (see the filled blue circles in Figs. 15 and 16), the two-peak Schottky-type anomaly behavior of the specific heat capacity emerges for well-defined intervals of the parameters for which the first-order single-point ground states exist (given by the corresponding lines in the plane $H/|J|$ versus α) from relatively close vicinity of the zero-order ground states (the dashed red lines in Figs. 15 and 16) along with the standard one-peak behavior of the specific heat capacity which is realized on the remaining parts of these lines (the solid blue lines in Figs. 15 and 16).

Finally, let us analyze the temperature properties of the specific heat capacity for the values of the parameters for which the second-order ground states, i.e., the plateau ground states, are realized. Here, detailed analysis shows that the third peak appears in the temperature dependence of the specific heat capacity when the parameters of the model belong to rather restricted but well-defined two-dimensional regions close simultaneously to lines and points for which the first-order and the zeroth-order single-point ground states exist [see the regions denoted by green roman numeral III in Fig. 16 (they can also be seen in Fig. 15, although they are not explicitly denoted there)]. Besides, when the chosen values of the parameters are such that the corresponding point in the plane $H/|J|$ versus α is far enough from one of the lower order ground states but, at the same time, close enough to the second one, then the specific heat capacity exhibits standard two-peak Schottky-type anomaly behavior (see the regions denoted by red roman numeral II in Figs. 15 and 16). Finally, the one-peak structure of the specific heat capacity as the function of the temperature is observed when the parameters of the model are chosen far enough from the values of the parameters for which all lower order ground states are realized (see the regions denoted by blue roman numeral I in Figs. 15 and 16).

The complete division of the plane $H/|J|$ versus α into the subregions where the specific heat capacity exhibits the one-peak, two-peak, and three-peak behavior as the function of the temperature is shown in detail in Figs. 15 and 16. As follows from Figs. 15 and 16, the parts of lines in the parameter space on which the first-order ground states are realized represent the separation lines between neighboring two-dimensional regions of parameters for which the second-order ground states exist (in our case, they are the regions with the maximal dimensions and therefore for them the plateau ground states are formed in the limit $T \to 0$) and for which the specific heat capacity has one more peak in comparison with the number of peaks on the corresponding parts of the lines (see the dashed red and solid blue lines and the corresponding neighboring regions in Figs. 15 and 16). At the same time, as also follows from these figures, the zeroth-order ground-state values of the parameters, for which the specific heat capacity has standard one-peak behavior, represent points which separate various regions with

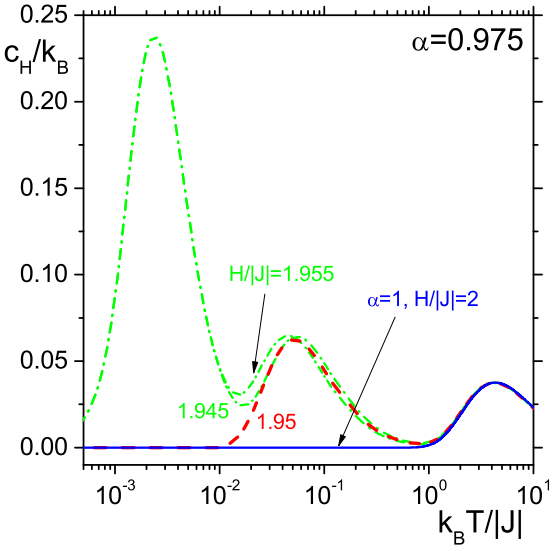

FIG. 17. The three-peak behavior of the specific heat capacity as the function of the temperature for $\alpha = 0.975$ in the left and right vicinity of the line $H/|J| = 2\alpha$ for which the corresponding first-order single-point ground state is formed in the limit $T \to 0$ (the dash-dotted green curves for $H/|J| = 1.945$ and 1.955). The corresponding two-peak curve for $H/|J| = 1.95$, i.e., for the value of the magnetic field directly on the first-order single-point ground-state line (the dashed red curve), as well as one-peak specific heat capacity curve for the zero-order single-point ground-state parameter values $H/|J| = 2$ and $\alpha = 1$ (the solid blue curve) are included for comparison.

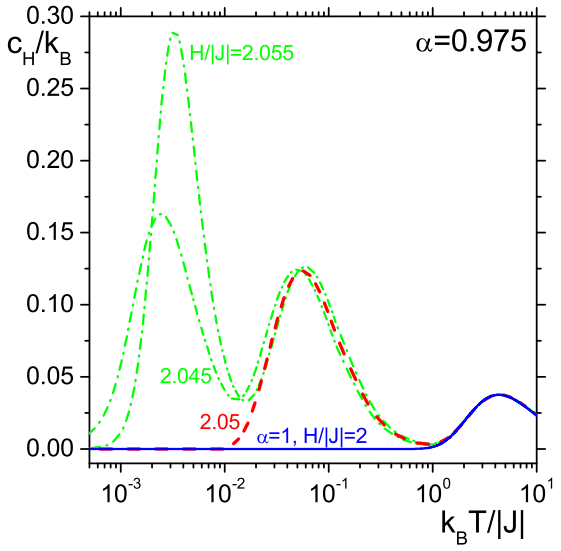

FIG. 18. The three-peak behavior of the specific heat capacity as the function of the temperature for the same value of the parameter $\alpha = 0.975$ in the left and right vicinity of the line $H/|J| = 4 - 2\alpha$ for which the corresponding first-order single-point ground state is formed in the limit $T \to 0$ (the dash-dotted green curves for $H/|J| = 2.045$ and 2.055). Again, the corresponding two-peak curve for $H/|J| = 2.05$, i.e., for the value of the magnetic field directly on the first-order single-point ground-state line (the dashed red curve), as well as one-peak specific heat capacity curve for the zero-order single-point ground-state parameter values $H/|J| = 2$ and $\alpha = 1$ (the solid blue curve) are included for comparison.

two-peak as well as three-peak structures in the temperature behavior of the specific heat capacity.

The existence of the three-peak structure in the behavior of the specific heat capacity is demonstrated explicitly in Figs. 17 and 18, where the specific heat capacity as a function of the reduced temperature is shown for $\alpha = 0.975$ and various values of the external magnetic field from the close vicinity of the point with $H/|J| = 2$ and $\alpha = 1$ for which the zeroth-order single-point ground state is realized as well as from the left and right vicinity of the lines $H/|J| = 2\alpha$ and $H/|J| = 4 - 2\alpha$, respectively, for which the corresponding first-order single-point ground states are formed in the limit $T \to 0$. As follows from Fig. 17, the heights of the third peaks of the specific heat capacity, i.e., the heights of the peaks which are realized for the lowest values of the temperature, are the same for the curves from the left and right vicinity of the parameter line $H/|J| = 2\alpha$. It is related to the fact that the neighboring plateau-ground states which are separated by the corresponding line of the single-point ground states have the same nonzero value of the residual entropy (see Fig. 6), which is also illustrated in Fig. 19. It is evident from this figure that, in this case, the dependence of the entropy on the temperature is very similar (see the dash-dotted green curves for $H/|J| = 1.945$ and 1.955 in Fig. 19). As follows from Fig. 19, the formation of the third peak in the behavior of the specific heat capacity is directly related to the nearby presence of the first-order single-point ground-state residual entropy of which is larger than the residual entropy of the corresponding neighboring plateau ground state (see the dashed red curve for $H/|J| = 1.95$ in Fig. 19). Namely, the nearby presence of this highly macroscopically degenerated lower-order ground state seriously influences the entropy behavior in its vicinity with appearance of noticeable slowing down of the entropy

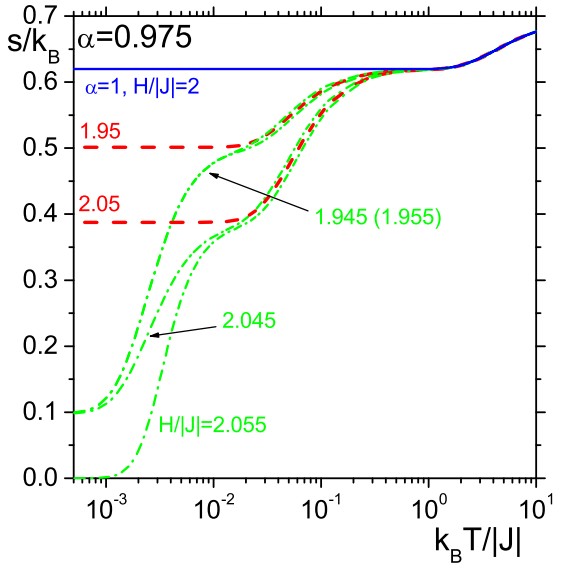

FIG. 19. The dependence of the entropy per site on the reduced temperature for $\alpha = 0.975$ and for the same values of the external magnetic field as in Figs. 17 and 18.

decreasing in an interval of the temperature with subsequent rapid change of the entropy when temperature decreases.

On the other hand, as follows from Fig. 18, the heights of the third peaks in the behavior of the specific heat capacity for the parameter values from the left and right vicinity of the line $H/|J| = 4 - 2\alpha$, for which the corresponding first-order single-point ground state is formed, are different. Here, it is related to the existence of considerable difference between residual entropies of the corresponding neighboring plateau-like ground states (see Fig. 6). The higher peak corresponds to the plateau ground state with lower residual entropy. At the same time, the origin of the formation of these peaks is completely the same as in the previous case, as it follows from the temperature dependence of the corresponding entropy curves in Fig. 19 (see the dash-dotted green curves for $H/|J| = 2.045$ and 2.055 as well as the dashed red curve for $H/|J| = 2.05$).

In the same manner, the very existence of the second peaks (the middle peak in the three-peak structure) in the behavior of the specific heat capacity as well as their heights (see Figs. 17 and 18) are directly related to the corresponding differences between residual entropies of the nearby first- and zeroth-order single-point ground states. Again, the influence of the existence of the zeroth-order single-point ground state on the entropy behavior in its vicinity is manifested in the steplike entropy behavior near the residual entropy value of the zeroth-order single-point ground state in an interval of temperatures (see Fig. 19). As also follows from Figs. 17 and 18, the second peak in the three-peak structure of the specific heat capacity is completely equivalent to the Schottky-peak in the two-peak structure of the specific heat capacity for the values of the parameters for which the first-order single-point ground state is realized (see the dashed red curves in Figs. 17 and 18). This behavior is a direct manifestation of the fact that all these peaks have the same origin described above.

Finally, the existence of a common standard first peak in the behavior of the specific heat capacity, which has the same properties for all values of the parameters from the vicinity of the zeroth-order single-point ground state (see Figs. 17 and 18), is directly related to the form of the entropy evolution between the entropy value which corresponds to the residual entropy of the zeroth-order single-point ground state and the maximal possible value of the entropy per site for any two-state system, namely, $s_{\max} = k_B \ln 2$.

The complexity of the low-temperature specific heat capacity behavior as the function of the external magnetic field in the vicinity of the zeroth-order and the corresponding first-order single-point ground states is explicitly shown in Fig. 20 for $\alpha = 0.975$. In Fig. 20, the formation of the second and third peaks in the temperature behavior of the specific heat capacity close to the first-order single point values of the external magnetic field, i.e., close to $H/|J| = 1.95$ and 2.05, can be seen. Note that the first standard peak in the specific heat capacity behavior is not present in Fig. 20 because it is realized for considerably higher temperatures (see Figs. 17 and 18). It is also important to note that, as immediately follows from Fig. 20, the field-induced double-peak structure in the specific heat capacity behavior occurs in the vicinity of each value of the external magnetic field where the first-order single-point ground state is formed in the limit $T \to 0$.

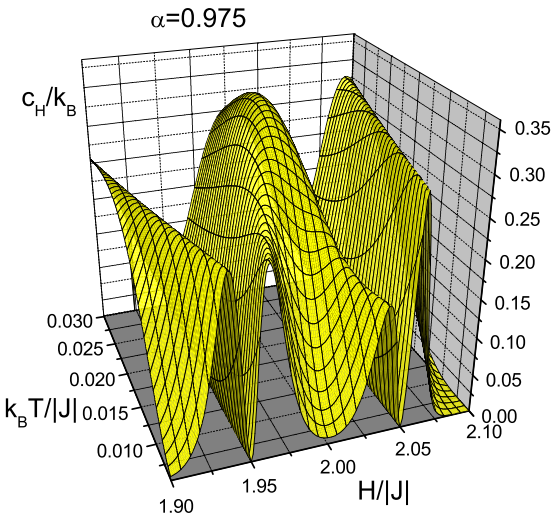

FIG. 20. The behavior of the low-temperature specific heat capacity for $\alpha = 0.975$ as the function of the values of the external magnetic field from the vicinity of the zeroth-order single-point ground state at the point $H/|J| = 2$ and $\alpha = 1$ as well as from the vicinity of the corresponding two first-order single-point ground states which are realized on the lines $H/|J| = 2\alpha$ and $H/|J| = 4 - 2\alpha$, respectively.

Typical temperature behavior of the specific heat capacity in the left and right vicinity of a first-order single-point ground state near the corresponding zeroth-order single-point ground state is demonstrated in Figs. 21 and 22 for the first-order single-point ground state which is realized for $H/|J| = 1.7$ and $\alpha = 0.85$ on the line $H/|J| = 2\alpha$ in the vicinity of the zeroth-order single-point ground state at the point $H/|J| = 2$ and $\alpha = 1$ (see Fig. 16). As follows from Fig. 21, depending on the value of the external magnetic field from the left vicinity

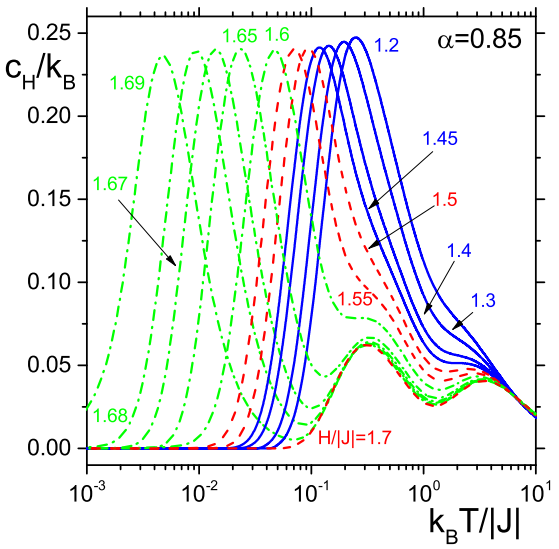

FIG. 21. One-peak (solid blue curves), two-peak (dashed red curves), and three-peak (dash-dotted green curves) temperature behavior of the specific heat capacity for various external magnetic field values from the left vicinity of the first-order single-point ground state which is realized at $H/|J| = 1.7$ and $\alpha = 0.85$ on the line $H/|J| = 2\alpha$ for $-1 < \alpha < 1$.

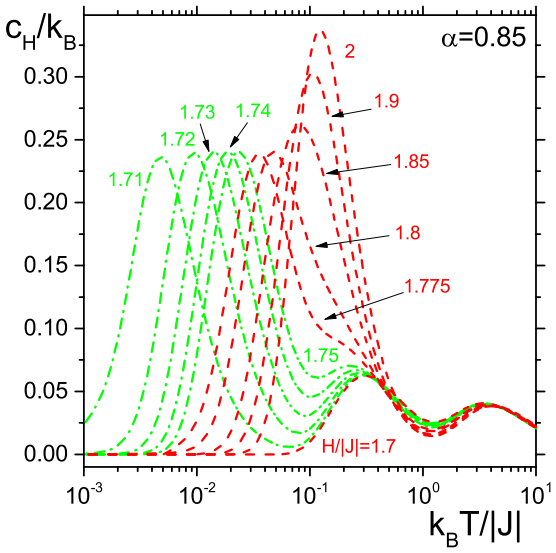

FIG. 22. Two-peak (dashed red curves) and three-peak (dash-dotted green curves) temperature behavior of the specific heat capacity for various external magnetic field values from the right vicinity of the first-order single-point ground state which is realized at $H/|J| = 1.7$ and $\alpha = 0.85$ on the line $H/|J| = 2\alpha$ for $-1 < \alpha < 1$.

of $H/|J| = 1.7$, the specific heat capacity exhibits one-peak, two-peak, and three-peak temperature behavior. On the other hand, in this case, as follows from Fig. 22, the specific heat capacity exhibits only two-peak and three-peak temperature behavior for the external magnetic fields from the right vicinity of the single-point value of the magnetic field $H/|J| = 1.7$. This is given by the fact that, in this case, the magnetic field values from the right vicinity of this single point belong only into the regions of the type II (dashed red curves) or III (dash-dotted green curves), as can be explicitly seen in Fig. 16. Let us note that similar temperature behavior of the specific heat capacity with one-peak, two-peak, and three-peak structure can be also obtained for the corresponding first-order single-point ground states on the red parts of the lines $H/|J| = \pm 4 - 2\alpha$ for $\alpha < 1$ and $\alpha > -1$ and $H/|J| = \pm 2$ for $\alpha > 1$ and $\alpha < -1$, respectively (see Figs. 15 and 16).

C. Multipeak structure of the specific heat capacity in frustrated magnetic systems

Detailed analysis of the specific heat capacity behavior performed in the previous sections in the framework of the studied geometrically frustrated magnetic system with two independent parameters allows us to generalize our main observations and conclusions to the frustrated magnetic systems with arbitrary number of independent parameters.

Our analysis shows that behavior of the specific heat capacity as the function of the temperature strictly depends on the existence of stepped hierarchies of the residual entropies (of the macroscopic degeneracies, respectively) of the system of the ground states of the model. In our case, in the framework of the model with two interactions J_1 and J_2 and the external magnetic field H one has two-dimensional ground-state parametric space defined by two independent parameters $H/|J_1|$ and $\alpha = J_2/|J_1|$ and the entire parametric space is divided into regions in which three different types of the ground states are realized: the zeroth-order (points), first-order (lines), and second-order ground states (two-dimensional regions). As shown in the previous section, in the zeroth-order ground-state parameter values, the specific heat capacity as the function of the temperature always exhibits only standard one-peak behavior. On the other hand, depending on the parameter values, the specific heat capacity exhibits standard one-peak behavior or two-peak Schottky-type anomaly behavior in the regions where the first-order ground states are realized. Finally, the specific heat capacity as the function of the temperature shows one-peak, two-peak, and three-peak anomalous behavior in the regions for which the second-order ground states are formed in the limit $T \to 0$. It means that for model parameters from the region of any ith-order ground state, one can see at most $i + 1$ peaks in the temperature behavior of the specific heat capacity. The actual number of peaks depends on the position in the parametric space of this ith-order ground state, as discussed in detail in the previous section and explicitly shown in Figs. 15 and 16.

Our conclusions obtained in the framework of the studied model can be directly generalized to arbitrary geometrically frustrated magnetic system with n interactions in the external magnetic field. Thus, suppose that one has an antiferromagnetic geometrically frustrated system with n different interactions $J_1, \ldots, J_n$ in the external magnetic field H. Then, as discussed in detail at the end of Sec. III, the independent ground-state parametric space of such a model is n dimensional and divided into i-dimensional regions $\mathcal{G}_{n,i}$ in which ith-order ground states are realized in the limit $T \to 0$. Therefore, by analogy with the studied model, depending on the parameter values, the specific heat capacity as the function of the temperature can exhibit at most $i + 1$ peaks for model parameters from regions which form $\mathcal{G}_{n,i}$. It also means that the maximal possible number of peaks in the temperature behavior of the specific heat capacity in the framework of such a model is $n + 1$. Of course, the maximal possible number of peaks can be realized only in the systems for which at least one complete strict hierarchy of the residual entropies of neighboring ground states of all orders exists. Note that in the model studied in this paper all residual entropy hierarchies are strict, i.e., the residual entropy of the lower-order ground state is always greater than the residual entropy of any neighboring ground state of higher order.

It is important to stress here that all our conclusions cannot be applied to the regions of parameters of a model for which the first-order phase transitions exist. There the situation is different and needs separate analysis.

From a phenomenological point of view, our analysis also allows us to make some conclusions for the experiment. Namely, if in general an n-peak temperature structure of the specific heat capacity is measured, then, from our pure theoretical analysis, it follows that the corresponding magnetic system is under influence of the hierarchical system of at least n residual entropies of neighboring ground states of different orders. In addition, it also automatically means that the ground-state parametric space of such a magnetic system must be at least n dimensional; i.e., the model must be driven at least by n different interactions (parameters). It means that a necessary condition for a theoretical model which would be

able to describe such a magnetic system is that it must take into account at least n different spin interactions.

Note that, as mentioned in the introduction, the nontrivial multipeak structures in the temperature behavior of the specific heat capacity are measured in real magnetic systems (see, e.g., Refs. [20–29] and many others). We suppose that present theoretical analysis can be considered as a well-defined starting point for fundamental understanding of the specific heat capacity behavior in such magnetic systems.

V. CONCLUSION

To conclude, let us briefly summarize the main results obtained in the present paper.

In this paper, we have investigated in detail anomalous properties of the specific heat capacity as the function of the temperature in frustrated magnetic systems in the framework of the geometrically frustrated exactly solvable antiferromagnetic spin-1/2 Ising model with multisite interaction in the presence of an external magnetic field on the kagome-like Husimi recursive lattice.

First, the exact expression for the free energy per site is used for investigation of the properties of the entropy per site of the model. The expression for the entropy is derived, the influence of the multisite interaction on its properties is discussed, and the residual entropies of all ground states of the model are determined. The existence of the ground states of different orders is demonstrated and it is shown that the model exhibits well-defined hierarchies of the macroscopic degeneracies of neighboring ground states of different orders.

The behavior of the specific heat capacity is then investigated in detail as the function of the temperature. First of all, depending on the parameter values, the specific heat capacity can exhibit at most a three-peak structure. The maximal number of peaks is directly related to the dimension of the corresponding ground-state parametric space of the model. The mechanism of the formation of the multipeak structure in the behavior of the specific heat capacity in the frustrated magnetic systems is identified. The central role for the formation of the multipeak structures in the behavior of the specific heat capacity is played by the existence of the nontrivial multilevel hierarchies of the residual entropies among various neighboring ground states of different orders. Obtained results are generalized to an arbitrary frustrated magnetic system with n independent spin interactions.

Although all results and conclusions are obtained only in the framework of a classical frustrated spin model, nevertheless we suppose that the described general mechanism of the formation of the multipeak structure in the specific heat capacity behavior will be valid, at least at a qualitative level, in many real frustrated magnetic systems.

ACKNOWLEDGMENTS

M.J. gratefully acknowledges the hospitality of the TH Division in CERN. This work was supported by VEGA Grant No. 2/0065/17 of Slovak Academy of Sciences and by the project ITMS No. 26220120029, based on the supporting operational research and development program financed by the European Regional Development Fund.

APPENDIX

The explicit expressions for the entropy per site s and the specific heat capacity c_H defined in Eqs. (2) and (16), respectively, have the following forms:

$$
\begin{aligned}
\frac{s}{k_B} = {} & [-3e^{2(7h+2K+K')}(h+6K+3K')x^7 - 3e^{12h}(h+6K+2K')x^6 + e^{14h+8K+4K'}(6h+24K+11K')x^6 \\
& - 2e^{4(3h+K+K')}[9h+5(6K+K')]x^6 - 3e^{2(5h+K')}(9h+26K-3K')x^5 - 8e^{10h+4K+6K'}(3h+6K-2K')x^5 \\
& + 4e^{12h+8K+6K'}(3h+6K-2K')x^5 - 4e^{2(5h+4K+K')}(3h+4K')x^5 + 2e^{2(6h+2K+K')}(12h+36K+13K')x^5 \\
& + 2e^{10h+4(K+K')}(33h+72K-4K')x^4 + 6e^{10h}(3h+2K-2K')x^4 - 54e^{8h+4K'}(h+2K-K')x^4 \\
& - 6e^{8(h+K)+4K'}(5h-2K+K')x^4 + e^{10h+12K+4K'}(6h-24K+5K')x^4 - 3e^{8h+4K}(7h-6K+6K')x^4 \\
& + 18e^{8h+2K'}(3h+2K-3K')x^3 - 24e^{6(h+K')}(h+2K-K')x^3 + 12e^{8h+4K+6K'}(3h+6K-K')x^3 \\
& - 8e^{6h+4K+2K'}(9h-6K+K')x^3 + 30e^{8(h+K)+2K'}(h-2K+K')x^3 - e^{2(3h+6K+K')}(9h-18K+7K')x^3 \\
& + 3e^{6h+4K'}(12h+8K-9K')x^2 - 2e^{4(h+K+K')}(21h-6K-K')x^2 + 2e^{6h+8K+4K'}[15h+4(K'-3K)]x^2 \\
& + 12e^{4h+6K'}K'x + 2e^{4(h+K)+2K'}(15h-18K+K')x - 3e^{2(h+4K+K')}(7h-10K+3K')x \\
& + 3e^{2[h+2(K+K')]}K' + (8e^{6h+4K}x^2 - 7e^{4h+8K}x^2 + 2e^{2(2h+6K+K')}x + 2e^{2h+8K} - e^{12K})(3h-6K+2K') \\
& + [-3e^{4h}x^2 + 2e^{2(h+K')}(-2+e^{2h+4K})x + 2e^{2h} - e^{4K}][e^{4h}x^2 + 2e^{2(h+K')}x + e^{4K}] \\
& \times [3e^{4h}x^2 + e^{2(h+K')}(e^{4(h+K)}x^2+3)x + e^{4K}](3\ln[e^{-2h-K-K'}(e^{4h}x^2 + 2e^{2(h+K')}x + e^{4K})] \\
& - \ln\{e^{-3h-K-K'}[3e^{4h}x^2 + e^{2(h+K')}(e^{4(h+K)}x^2+3)x + e^{4K}]\})]/ \\
& \{3[-3e^{4h}x^2 + 2e^{2(h+K')}(-2+e^{2h+4K})x + 2e^{2h} - e^{4K}][e^{4h}x^2 + 2e^{2(h+K')}x + e^{4K}] \\
& \times [3e^{4h}x^2 + e^{2(h+K')}(e^{4(h+K)}x^2+3)x + e^{4K}]\},
\end{aligned}
$$

$$\frac{c_H}{k_B} = e^{2h}[3e^{18h+8K+4K'}(Bx-A^2)\beta^2x^8 + 3e^{2(8h+2K+K')}\{-4(h+2K+K')^2x^2 - 4A(h+2K+K')\beta x$$
$$+ 2e^{4(K+K')}[4x(h-K')^2 + 4A\beta(h-K') + B\beta^2]x + (7Bx-8A^2)\beta^2\}x^7 + 12e^{14h}\{-3(A^2-Bx)\beta^2$$
$$+ e^{4(3K+K')}(2hx-2Kx+A\beta)^2 - e^{4(K+K')}[4(-h^2+6Kh+8K'h+5K^2-2K'^2+4KK')x^2$$
$$- 4A(h-3K-4K')\beta x + (5A^2-6Bx)\beta^2]\}x^6 + e^{2(6h+K')}(-24e^{4(K+K')}[4(h^2+6Kh+4K'h+4K^2-K'^2$$
$$+ 2KK')x^2 + 4A(h+3K+2K')\beta x + (4A^2-3Bx)\beta^2] + 6e^{4(3K+K')}[4(h-2K+K')^2x^2$$
$$+ 4A(h-2K+K')\beta x + (2A^2-Bx)\beta^2] + e^{8K}\{4[57h^2-6(28K+3K')h+48K^2-7K'^2-24KK']x^2$$
$$+ 12A(19h-28K-3K')\beta x + 3(14A^2+5Bx)\beta^2\} + 9[20(h-K')^2x^2 + 20A(h-K')\beta x + (19Bx$$
$$- 14A^2)\beta^2])x^5 + e^{10h}(-24e^{4K+8K'}[8(h+K)^2x^2 + 8A(h+K)\beta x + (3A^2-Bx)\beta^2] + 48e^{4K}[8(h-K)^2x^2$$
$$+ 8A(h-K)\beta x + (A^2+Bx)\beta^2] + e^{4K'}\{3e^{16K}(A^2-Bx)\beta^2 + 4e^{8K}[16(3h^2-24Kh+9K^2+2K'^2$$
$$- 12KK')x^2 + 48A(h-4K)\beta x + 3(3A^2+Bx)\beta^2] + 9[32(h-K')^2x^2 + 32A(h-K')\beta x$$
$$+ (33Bx-25A^2)\beta^2]\})x^4 + e^{8h+2K'}(16e^{8K+4K'}[-4(3h^2+15Kh-3K'h-6K^2-2K'^2+9KK')x^2$$
$$+ 6A(-2h-5K+K')\beta x - 3A^2\beta^2] + e^{12K}\{4[-5K'^2-6(3h+2K)K'+3(h^2-20Kh+4K^2)]x^2$$
$$+ 12A(h-10K-3K')\beta x + 3(4A^2-3Bx)\beta^2\} + 18e^{4K'}[4(h-K')^2x^2 + 4A(h-K')\beta x + (13Bx-12A^2)\beta^2]$$
$$+ 3e^{4K}[4(79h^2-180Kh+22K'h+124K^2+23K'^2-68KK')x^2 + 4A(79h-90K+11K')\beta x$$
$$+ (28A^2+51Bx)\beta^2])x^3 - 4e^{6h}(18e^{8K'}(A^2-Bx)\beta^2 + e^{4(3K+K')}[4(9h^2+18Kh-9K^2-2K'^2+12KK')x^2$$
$$+ 36A(h+K)\beta x + 3(2A^2+Bx)\beta^2] - 3e^{8K}[16(h-K)^2x^2 + 16A(h-K)\beta x + (3A^2+Bx)\beta^2]$$
$$- 3e^{4(K+K')}\{4[13h^2-42Kh+37K^2+8K'^2+16(h-2K)K']x^2 + 4A(13h-21K+8K')\beta x$$
$$+ (15Bx-2A^2)\beta^2\})x^2 + e^{4(h+K)+2K'}\{-e^{12K}[4(3h+K')^2x^2 + 12A(3h+K')\beta x + 3(2A^2+Bx)\beta^2]$$
$$+ 3e^{4K}[4(17h^2-56Kh+22K'h+48K^2+9K'^2-40KK')x^2 + 4A(17h-28K+11K')\beta x + (6A^2+11Bx)\beta^2]$$
$$+ 6e^{4K'}[28(h-2K+K')^2x^2 + 28A(h-2K+K')\beta x + (13Bx-6A^2)\beta^2]\}x + 3e^{2(6K+K')}\big[4x(h-2K+K')^2$$
$$+ 4A\beta(h-2K+K') + B\beta^2\big] + 3e^{2h+8K+4K'}[32(h-2K+K')^2x^2 + 32A(h-2K+K')\beta x$$
$$- (A^2-9Bx)\beta^2]]/[3(2xe^{2h+2K'} + e^{4h}x^2 + e^{4K})^2(x^3e^{6h+4K+2K'} + 3xe^{2h+2K'} + 3e^{4h}x^2 + e^{4K})^2],$$

where

$$A = \{-x^2e^{4(h+K)+2K'}[4(h+K)+K'] + e^{4h}x^3(4h-K') + 2x^2e^{2(h+K')}(2h+K') + 2e^{2h}x(K'-2h)$$
$$+ e^{4K}x(4K-K') - e^{2K'}K'\}/\{\beta[2x(e^{2h+4K}-2)e^{2(h+K')} - 3e^{4h}x^2 + 2e^{2h} - e^{4K}]\},$$
$$B = \{-e^{4(h+K)+2K'}[2A^2\beta^2 + 4A\beta x(4h+4K+K') + x^2(4h+4K+K')^2]$$
$$+ 2e^{2(h+K')}[2A^2\beta^2 + 4A\beta x(2h+K') + x^2(2h+K')^2] + e^{4h}x\big[6A^2\beta^2 + 6A\beta x(4h-K') + x^2(K'-4h)^2\big]$$
$$- 2e^{2h}(2h-K')(2A\beta + 2hx - K'x) + e^{4K}(4K-K')(2A\beta + 4Kx - K'x) - e^{2K'}K'^2\}/$$
$$\{\beta^2[2x(e^{2h+4K}-2)e^{2(h+K')} - 3e^{4h}x^2 + 2e^{2h} - e^{4K}]\},$$

and x is given in Eq. (4).

[1] A. P. Ramirez, Annu. Rev. Mater. Sci. **24**, 453 (1994).
[2] N. P. Raju, E. Gmelin, and R. K. Kremer, Phys. Rev. B **46**, 5405 (1992).
[3] K. Ishida, M. Morishita, K. Yawata, and H. Fukuyama, Phys. Rev. Lett. **79**, 3451 (1997).
[4] V. K. Pecharsky and K. A. Gschneidner, Jr., Phys. Rev. Lett. **78**, 4494 (1997).
[5] M. J. Harris, S. T. Bramwell, P. C. W. Holdsworth, and J. D. M. Champion, Phys. Rev. Lett. **81**, 4496 (1998).
[6] N. P. Raju, M. Dion, M. J. P. Gingras, T. E. Mason, and J. E. Greedan, Phys. Rev. B **59**, 14489 (1999).
[7] R. Siddharthan, B. S. Shastry, A. P. Ramirez, A. Hayashi, R. J. Cava, and S. Rosenkranz, Phys. Rev. Lett. **83**, 1854 (1999).
[8] R. G. Melko, B. C. den Hertog, and M. J. P. Gingras, Phys. Rev. Lett. **87**, 067203 (2001).
[9] K. Matsuhira, Z. Hiroi, T. Tayama, S. Takagi, and T. Sakakibara, J. Phys.: Condens. Matter **14**, L559 (2002).
[10] Z. Hiroi, K. Matsuhira, S. Takagi, T. Tayama, and T. Sakakibara, J. Phys. Soc. Jpn. **72**, 411 (2003).
[11] Z. Hiroi, K. Matsuhira, and M. Ogata, J. Phys. Soc. Jpn. **72**, 3045 (2003).
[12] S. S. Sosin, L. A. Prozorova, A. I. Smirnov, A. I. Golov, I. B. Berkutov, O. A. Petrenko, G. Balakrishnan, and M. E. Zhitomirsky, Phys. Rev. B **71**, 094413 (2005).
[13] X. Ke, M. L. Dahlberg, E. Morosan, J. A. Fleitman, R. J. Cava, and P. Schiffer, Phys. Rev. B **78**, 104411 (2008).

[14] X. Ke, D. V. West, R. J. Cava, and P. Schiffer, Phys. Rev. B **80**, 144426 (2009).
[15] J. S. Gardner, M. J. P. Gindras, and J. E. Greedan, Rev. Mod. Phys. **82**, 53 (2010).
[16] S. Pakhira, C. Mazumdar, R. Ranganathan, S. Giri, and M. Avdeev, Phys. Rev. B **94**, 104414 (2016).
[17] E. V. Shevchenko, E. V. Charnaya, M. K. Lee, L. J. Chang, E. N. Khazanov, A. V. Taranov, and A. S. Bugaev, Phys. Lett. A **381**, 330 (2017).
[18] J. Brambleby, P. A. Goddard, J. Singleton, M. Jaime, T. Lancaster, L. Huang, J. Wosnitza, C. V. Topping, K. E. Carreiro, H. E. Tran, Z. E. Manson, and J. L. Manson, Phys. Rev. B **95**, 024404 (2017).
[19] S. Lucas, K. Grube, C.-H. Huang, A. Sakai, W. Wunderlich, E. L. Green, J. Wosnitza, V. Fritsch, P. Gegenwart, O. Stockert, and H. v. Löhneysen, Phys. Rev. Lett. **118**, 107204 (2017).
[20] B. Revaz, A. Junod, and A. Erb, Phys. Rev. B **58**, 11153 (1998).
[21] A. P. Ramirez, A. Hayashi, R. J. Cava, R. Siddharthan, and B. S. Shastry, Nature (London) **399**, 333 (1999).
[22] S. Noguchi, T. Sakon, H. Nojiri, and M. Motokawa, Phys. B (Amsterdam, Neth.) **346–347**, 179 (2004).
[23] S. Noguchi, T. Sakon, H. Nojiri, and M. Motokawa, Phys. B (Amsterdam, Neth.) **346–347**, 183 (2004).
[24] L. Gondek, A. Szytula, D. Kaczorowski, A. Szewczyk, M. Gutowska, and P. Piekarz, J. Phys.: Condens. Matter **19**, 246225 (2007).
[25] P. Schobinger-Papamantellos, J. Rodríguez-Carvajal, L. D. Tung, C. Ritter, and K. H. J. Buschow, J. Phys.: Condens. Matter **20**, 195201 (2008).
[26] D. O'Flynn, M. R. Lees, and G. Balakrishnan, J. Phys.: Condens. Matter **26**, 256002 (2014).
[27] I. Panneer Muthuselvam, R. Sankar, A. V. Ushakov, W. T. Chen, G. Narsinga Rao, S. V. Streltsov, S. K. Karna, L. Zhao, M.-K. Wu, and F. C. Chou, J. Phys.: Condens. Matter **27**, 456001 (2015).
[28] D. Villundas, T. Tsutaoka, and J. M. Hernàndes Ferràs, J. Magn. Magn. Mater. **405**, 282 (2016).
[29] M. Ito, T. Furuta, K. Kai, A. Taira, K. Onda, I. Shigeta, and M. Hiroi, J. Magn. Magn. Mater. **428**, 390 (2017).
[30] L. Zhong, X. Wang, M. Rong, and Y. Cressault, Eur. Phys. J. D **70**, 233 (2016).
[31] B. M. McCoy and T. T. Wu, *The Two-Dimensional Ising Model* (Harvard University Press, Cambridge, MA, 1973).
[32] R. J. Baxter, *Exactly Solved Models in Statistical Mechanics* (Academic Press, London, 1982).
[33] H. T. Diep (ed.) *Frustrated Spin Systems* (World Scientific, Singapore, 2004).
[34] X. N. Wu and F. Y. Wu, J. Phys. A: Math. Gen. **22**, L1031 (1989).
[35] G. Toulouse, Commun. Phys. **2**, 115 (1977).
[36] K. Husimi, J. Chem. Phys. **18**, 682 (1950).
[37] F. Harary and G. E. Uhlenbeck, Proc. Nat. Acad. Sci.: USA **39**, 315 (1953).
[38] J. W. Essam and M. E. Fisher, Rev. Mod. Phys. **42**, 272 (1970).
[39] L. Monroe, J. Stat. Phys. **65**, 255 (1991).
[40] L. Monroe, J. Stat. Phys. **67**, 1185 (1992).
[41] J. L. Monroe, Phys. A (Amsterdam, Neth.) **256**, 217 (1998).
[42] M. Pretti, J. Stat. Phys. **111**, 993 (2003).
[43] N. S. Ananikian, V. V. Hovhannisyan, and H. A. Lazaryan, Int. J. Mod. Phys. B **24**, 5913 (2010).
[44] E. Jurčišinová, M. Jurčišin, and A. Bobák, Phys. Lett. A **377**, 2712 (2013).
[45] E. Jurčišinová, M. Jurčišin, and A. Bobák, J. Stat. Phys. **154**, 1096 (2014).
[46] E. Jurčišinová and M. Jurčišin, Phys. Rev. E **89**, 032123 (2014).
[47] N. S. Ananikian, N. Sh. Izmailian, and K. A. Oganessyan, Phys. A (Amsterdam, Neth.) **254**, 207 (1998).
[48] P. D. Gujrati, Phys. Rev. Lett. **74**, 809 (1995).
[49] E. Jurčišinová and M. Jurčišin, Phys. A (Amsterdam, Neth.) **486**, 296 (2017).
[50] K. Kanô and S. Naya, Prog. Theor. Phys. **10**, 158 (1953).
[51] Yu. I. Dublenych, Phys. Rev. E **84**, 061102 (2011).
[52] Yu. I. Dublenych, Phys. Rev. Lett. **109**, 167202 (2012).
[53] Yu. I. Dublenych, Phys. Rev. E **88**, 022111 (2013).
[54] Yu. I. Dublenych, J. Phys.: Condens. Matter **25**, 406003 (2013).